

Flow of Granular Material Through a Plane Hopper

R. L. MICHALOWSKI*

University of Minnesota, Department of Civil and Mineral Engineering, 500 Pillsbury Drive, S.E., Minneapolis, MN 55455 (U.S.A.)

(Received May 23, 1983; revised for October 10, 1983)

SUMMARY

This paper presents some experimental results of an investigation of flow patterns of sand in a plane, wedge-shaped hopper model and also an approach to a theoretical description of the discharge process. A non-steady discontinuous velocity field was observed in the experiments. Velocity discontinuities were traced during the process of discharge using the stereophotographic technique. Complementary information about the density variations of the material during discharge was obtained from X-ray pictures and from ultrasonic measurements.

Theoretical description of the velocity field is restricted to the advanced flow, which, as demonstrated in the experiments, can be treated approximately as a pseudo-steady process. An approach based upon the plane plastic flow theory of incompressible Coulomb material is applied. The theoretical solution for the velocity field is compared with some of the experimental results.

INTRODUCTION

The paper consists of two parts. In the first one, the flow through a plane, wedge-shaped hopper model is experimentally investigated. The stereophotographic technique is used in order to determine the location of any disturbances in the velocity field. Variation of the density of the material during flow is described making use of unpublished results of X-ray experiments performed by A. Drescher at the University of Cambridge in 1976. The ultrasonic method of density

measurement is also used in order to obtain some quantitative results. The second part of the paper is devoted to mathematical description of the advanced stage of flow, based on the plane plastic flow theory.

Experiments on gravitational flow of granular material through hoppers have been carried out by many investigators: Pariseau [1], Blair-Fish and Bransby [2, 3], Lee, Cowin and Templeton [4], Nedderman and Tüzün [5, 6], and others. A large number of experiments have shown that narrow zones of large deformation, called here after Blair-Fish and Bransby [2], the rupture surfaces, occur within the flowing regions. Large shearing strains are accompanied by dilation of the material. Velocities of the particles experience a rapid variation across the rupture surfaces, hence they are often interpreted as velocity discontinuities. No discontinuities in the velocity field were observed by Nedderman and Tüzün [5]; however, their experiments differ markedly from those of Pariseau [1], Bransby and Blair-Fish [2, 3], and also from those presented in this paper.

The aim of experiments presented in this paper is to determine the flow patterns (the rupture surfaces in particular) during the entire discharge process rather than the velocity field at one particular moment of the flow.

Three different approaches to a theoretical description of the velocity distribution in hoppers can be distinguished. The first one is based on plasticity theory, in which the stress distribution is first calculated and then the boundary problem for velocities solved (Shield [7, 8], Jenike [9], Spencer [10], Pariseau [1]). The second approach, presented by Drescher, Cousens and Bransby [11], is also based on plasticity theory; however, the kinematically admissible velocity field is

*University of Minnesota, on sabbatical leave from the Technical University of Poznań, Poland.

obtained without predicting the stress field. This is possible by assuming *a priori* the pattern of the velocity field. The third approach involves a purely kinematic model, developed mainly by Litwiniszyn [12] and Mullins [13, 14], and successfully applied to the problem of flow through hoppers by Nedderman and Tüzün [5, 6]. This model was suggested by Nedderman and Tüzün [5] solely for steady flow of a dilated material.

In the present paper, the first approach is applied. The radial stress field [9] is adopted here and then the velocity boundary problem solved for boundary conditions defined from the experiments. Referring to the experimental results, it is suggested that pseudo-steady flow occurs in the advanced stage of flow.

Theoretical description based on similar assumptions was given earlier by Pariseau [1]. However, the principal strain-rate trajectories were determined by Pariseau experimentally, and the problem for velocities was solved for boundary conditions different from those proposed here. The objective of the theoretical investigation presented in this paper was to describe the flow without a large number of experimental data. Experimental results were used, however, in order to determine the boundary conditions.

HOPPER MODEL AND EXPERIMENTAL TECHNIQUES

The experiments presented here, except for the X-ray investigations, were performed on a model of the plane hopper built in the Institute of Fundamental Technological Research in Warsaw. The hopper model consisted of two wooden bars (hopper walls), each 4 cm thick and 85 cm long, placed between two glass sheets. Some introductory experiments were compared with those performed on models with larger ratios of the thickness to the distance between the hopper walls (e.g. [3, 15, 16]), in which the flow patterns were investigated by means of the X-ray technique. The results allow one to believe that in the experiments presented in this paper the side friction from the glass did not influence the flow patterns in any significant way. The inclination of the walls

and the width of the outlet could be adjusted according to the program of experiments. Sand with particle diameters in the range of 0.25 - 1.75 mm was used in all experiments. Initial density ρ_0 of the material placed in the hopper for different experiments varied from 1.55 to 1.70×10^3 kg/m³. In order to produce low and high wall friction, the hopper walls were covered with oil paint (wall friction angle $\phi_w = 11^\circ$) or sand paper ($\phi_w = 25^\circ$). In experiments where the density was measured by means of the ultrasonic method, the glass sheets were replaced by Plexiglas and the ultrasonic heads were inserted into the holes drilled into the Plexiglas. X-ray experiments were performed in a similar Plexiglas hopper model built in Cambridge.

Stereo-photographic technique

Stereo-photogrammetry provides a powerful method for measuring planar displacement (or velocity) fields. The method was discussed in detail by Butterfield, Harkness and Andrawes [17]. The stereo-photographic technique seems to be particularly suitable for investigating any disturbance in the velocity field. Here it is expected to supply information about propagation of the rupture surfaces. It is clearly understood that the stereoscopic image obtained from the pictures of the material flowing through the hopper, in time t and $t + \delta t$, is related not only to the velocity field at time t but also, due to non-steady flow, to the variation of the velocity field in the time increment δt . This variation can usually be neglected for the flow regions where the velocity field is continuous and for small increments δt . Finally, the field of displacements can be interpreted as a velocity field. The stereoscopic image of displacements has to be interpreted more carefully, however, if the discontinuities appear in the velocity field. The discontinuity in a steady velocity field in a stereoscopic image is seen as a 'slope' rather than a vertical 'fault'. The width of the 'slope' depends on the time increment, but its inclination does not. In the real case of flow of granular material through hoppers, the discontinuities move with their own velocities. It is possible to define the velocity of propagation of the discontinuity lines using the stereophotographic technique together with some direct measurements on the photographs.

Although the stereo-photographic method was used mainly to trace the development of the rupture surfaces, it was also used to identify the selected particles on the photographs, so the displacement vectors could be obtained from direct measurements.

Radiographic technique

The radiographic technique was used in order to investigate a variation of density of the material during flow through the hopper model. The X-radiographs were taken while the flow was stopped. Due to variation of X-ray attenuation with the density of the material, the X-ray shadow shows clearly the areas of dense (dark) and loose (light) material. The radiographic technique was applied earlier to the problem of flow through hoppers by many investigators [2, 4, 15, 16]. The X-ray technique was used here solely to investigate the density; however, it can be also used to measure strains [18].

Ultrasonic technique of density measurement

The ultrasonic technique was used on a small scale to obtain some supplementary quantitative results of density variation. This technique uses the relation between the velocity of a longitudinal elastic wave and the density of the material. The time during which the wave crossed the material placed in the hopper model was measured (for stopped flow) and then converted into the wave velocity, and finally the density of the material was computed from the empirical relation between the density and the wave velocity. The velocity of wave propagation, however, is also a function of stress state, moisture content and grain characteristics, such as the diameter of particles, number of contacts per particle and the mechanical properties of the particles [19]. Therefore the empirical relations were obtained from a number of tests in which the variables considered were density and confining pressure $\sigma_{ii}/3$. All experiments were performed under the same humidity conditions. It was found for a given sand that for the confining pressure $\sigma_{ii}/3$ changing from 0 to about 2 kN/m², the influence of this pressure on wave velocity is negligible. Estimations of the stress state within the material placed in the hopper model gave the value of $\sigma_{ii}/3$ not exceeding 2 kN/m². Hence, for all experiments, the

density was computed from one empirical relation between density and velocity.

Since the ultrasonic technique of density measurement requires permanent location of the ultrasonic heads, the density of some characteristic areas cannot be traced during unsteady flow through the hopper. The measurements can be considered as reliable if the density of the area covered by the heads is uniform. Otherwise, the digitally registered time of wave propagation (across the model) corresponds to that part of the material (covered by the ultrasonic heads) in which the velocity of wave propagation is the highest. For the tested material, in the range of $\sigma_{ii}/3$ from 0 to about 9 kN/m², the velocity was higher for lower densities (as opposed to cases where $\sigma_{ii}/3 > 9$ kN/m²). Hence, in the experiments presented, the ultrasonic method underestimates the density if it is non-uniform.

The technique itself and obtained empirical relations were discussed in detail by Drescher and Michalowski [20].

EXPERIMENTAL RESULTS

The aim of the experiments was to describe flow patterns during the whole cycle of emptying the hopper. Although various experimental techniques were used, the overall picture will be reported in this section.

Two stages of the flow of granular material through plane hoppers can be distinguished: initial and advanced. Unsteady flow occurs in both of them. It will be shown, however, that the advanced flow can be interpreted as a pseudo-steady process and a fairly simple approximate theoretical description can be applied.

Initial flow

Two different mechanisms may appear in the initial stage of flow. In the first one, called here the *mass mechanism*, after the outlet of the hopper is open, two narrow, usually symmetrical, curvilinear zones of large deformation (rupture surfaces) occur in the neighbourhood of the outlet. The two rupture surfaces propagate gradually upward, cross in the vicinity of the axis of symmetry of the hopper and then reach the walls. The next pair of rupture surfaces starts then to 'grow'

from the vicinity of the points where the first pair reached the walls. Gradually more and more material starts to move as the rupture surfaces expand. The process is repeated until the rupture surfaces meet the top boundary of the material. While the process of propagation of the rupture surfaces progresses in the upper part of the hopper, the surfaces in the lower part move down, though they still remain as disturbances (discontinuities) within the velocity field. Propagation of the rupture surfaces in a hopper with the half-angle $\theta_w = 15^\circ$ ($\phi_w = 11^\circ$, $\rho_0 = 1.6 \times 10^3 \text{ kg/m}^3$) is shown in Fig. 1. The pattern of rupture surfaces was obtained by means of the stereoscopic technique. The rupture surfaces seen indistinctly in the stereoscopic image are marked by the broken lines.

After the large deformation zones reach the top boundary of the material in the hopper, the flow pattern becomes irregular and no clear sequence of events can be drawn until the free boundary of the material and the rupture surfaces are shaped as shown in Fig. 1g). This moment is considered here to be the end of the initial mass mechanism.

The top boundary of the material placed in the hopper starts to move down shortly after the outlet is open, but not at the exact same time. For this reason, the material is expected to dilate. Variation of the density in the initial mass mechanism is manifested by a variation of X-ray shadow on a sequence of X-radiographs^a in Fig. 2. The material dilates while passing the rupture surfaces, and a distinct dilation effect appears on the X-radiographs along these surfaces. The initially uniform density of the material becomes non-uniform and the patches of initially dense material gradually decrease.

The second mechanism that can occur in the initial stage of flow is called here a *plug mechanism*. In this case, after the process of emptying the hopper is initialized, material starts to move down only in a narrow zone separated from the stationary (dead) zones by two approximately vertical surfaces. Shortly after the outlet of the hopper is open, the plug zone reaches the free boundary of the material and expands sideways, so the dead

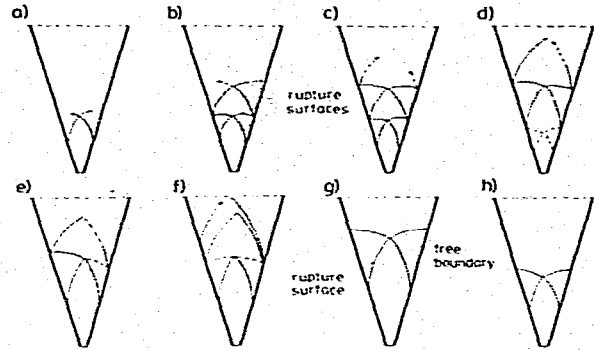


Fig. 1. Rupture surfaces in the initial mass mechanism (a - f)) and during the advanced flow (g, h)).

zones are gradually reduced. Besides the two clear surfaces separating the plug zone from the dead zones, some rupture surfaces occur within the upper and lower part of the plug zone. Expansion of the plug zone seen in the sequence of stereoscopic images is shown in Fig. 3a) - f). The experiment was carried out in a hopper model with the half-angle $\theta_w = 15^\circ$, $\phi_w = 11^\circ$, and for the initial density of the material $\rho_0 = 1.7 \times 10^3 \text{ kg/m}^3$. The initial stage of flow is considered to be completed when the dead zones are completely reduced. For some cases, particularly for large θ_w and rough walls, the duration of the plug mechanism may be quite long. A sequence of X-radiographs of the plug flow mechanism is shown in Fig. 4. It is seen that dilation of the material occurs along the vertical surfaces separating the plug zone from the dead zones. Hence, the density of the material within the plug zone is lower than that in the dead zones.

Occurrence of the mass or plug mechanism in the initial stage of flow depends on the geometry of the hopper, wall friction and parameters of the material. Even though a criterion of mass/plug flow was not derived, it is clear that the plug mechanism is likely to occur for relatively high wall friction and/or density of the material.

Advanced stage of flow

The advanced stage of flow is considered to begin when the entire material placed in the hopper starts to flow and the top boundary and rupture surfaces are shaped similarly as shown in Fig. 1g) and Fig. 3g). The velocity

^aThe upper edges of the hopper in Figs. 2 and 4 were cut out of the X-radiographs due to the size of the X-ray film.

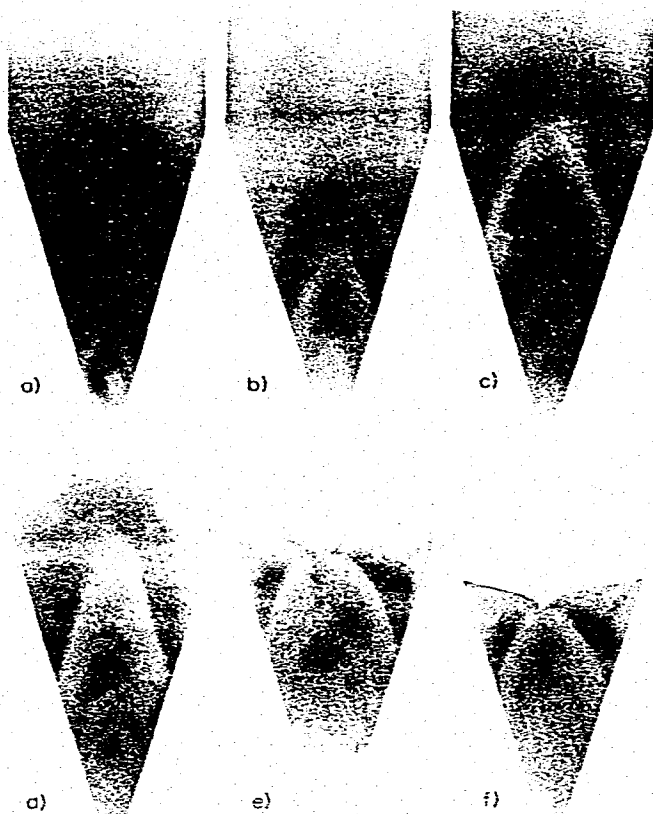


Fig. 2. X-radiographs of the initial mass mechanism (a - d)) and the advanced flow (e, f)) in a wedge-shaped hopper.

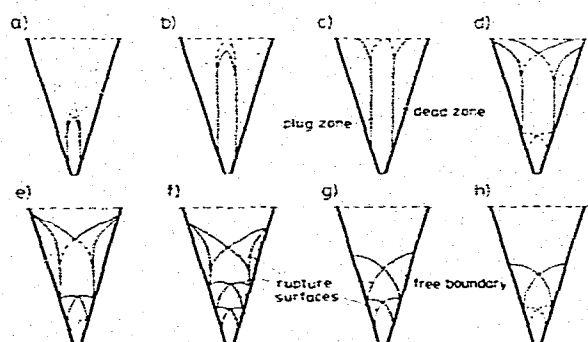


Fig. 3. Rupture surfaces in the initial plug mechanism (a - f)) and during the advanced flow (g, h)).

jump across the highest-located pair of rupture surfaces is relatively large, so these surfaces are very distinct in the stereoscopic image. The rupture surfaces below are sometimes hardly visible since the velocity jump

across them is relatively small. A characteristic feature of the advanced flow is that the discontinuities (rupture surfaces) in the upper part of the velocity field, where they are distinctly visible, remain geometrically similar until the very last stage of flow. This feature does not depend on whether the mass or plug mechanism occurred initially. Figure 5 shows the normalized shape of discontinuity lines for three different times of the advanced process ($\theta_w = 15^\circ$, $\phi_w = 11^\circ$, $\rho_0 = 1.6 \times 10^3 \text{ kg/m}^3$). It was found that the shape of discontinuities depends on the wall friction (see also [16]), but does not depend on the width of the outlet. Displacement increment vectors, measured experimentally, indicate that the curvilinear triangular regions ABC and A'BC' (Fig. 5a)) move parallel to the walls, approximately as rigid bodies (see also [11]). The measurements of the velocity field indicate slight departures from symmetry due to imperfections in the initial

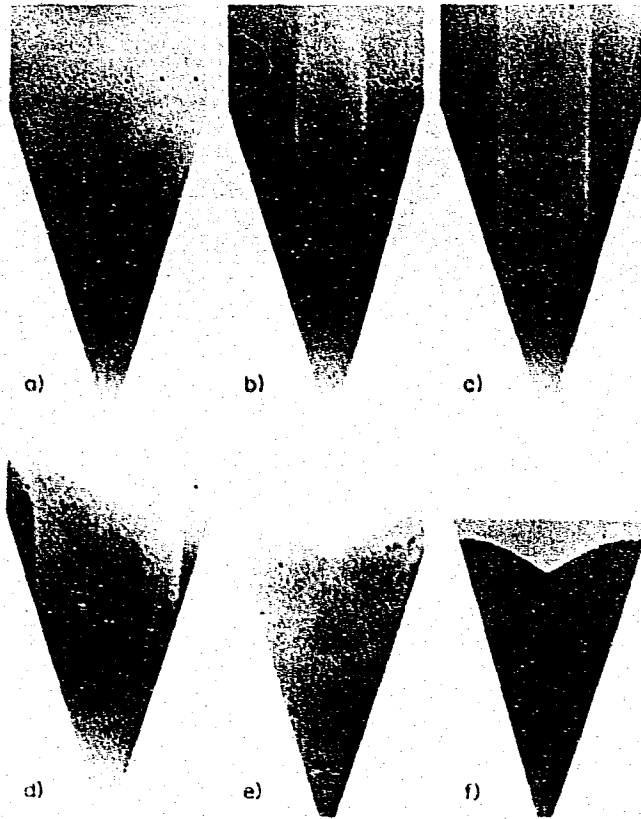


Fig. 4. X-radiographs of the initial plug mechanism (a - d)) and the advanced flow (e, f)) in a wedge-shaped hopper.

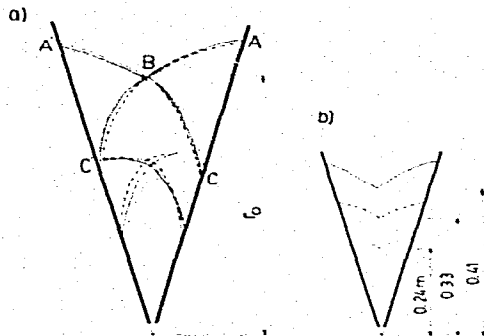


Fig. 5. Normalized image of rupture surfaces (a)) for three moments of the advanced stage of flow (b)).

distribution of density. They appear, however, to be of minor importance.

Geometrical similarity of rupture surfaces and rigid motion of the region ABC ($A'BC'$) in the advanced stage of flow will be important features used in the theoretical description.

Variation of the density in the advanced flow preceded by the initial mass mechanism is represented in X-radiographs in Fig. 2e) and f). The density is fairly uniform below the highest located pair of discontinuities. There are two patches of relatively dense material above them (in the areas of rigid motion). This material loosens progressively when passing from the rigid-motion regions to the area below. Hence, the first pair of discontinuity lines (the highest one) is still considered to be dilational, while the flow field below is approximately incompressible. Ultrasonic measurements of density in the area of rigid motion and below, however, do show very small differences, e.g. for the initial density $\rho_0 = 1.55 \times 10^3 \text{ kg/m}^3$ ($\theta_w = 15^\circ$, $\phi_w = 11^\circ$), the density during advanced flow in the incompressible field was $1.49 \times 10^3 \text{ kg/m}^3$, while the material above had a density practically equal to the initial one. For the same hopper model and higher

densities, plug flow was initially observed. Ultrasonic measurements of density in a model with $\theta_w = 10^\circ$ ($\phi_w = 11^\circ$) for initial densities $1.56, 1.63$ and $1.70 \times 10^3 \text{ kg/m}^3$ yield $1.50, 1.50$ and $1.51 \times 10^3 \text{ kg/m}^3$, respectively, in the advanced flow in the incompressible field, and in the rigid-motion area: $1.54, 1.55$ and $1.57 \times 10^3 \text{ kg/m}^3$, respectively. The significant drop of density in rigid-motion areas with respect to the initial one is due to the dilation in the initial stage of flow. The density of the material in the advanced flow preceded by the plug mechanism seems to be more uniform (Fig. 4e) and f); however, a weak dilation effect along the rupture surfaces can still be recognized. In this case, the entire material first loosened in the initial stage of flow due to expansion of the plug zone. Ultrasonic measurements again show very small differences in density. In the experiment where the initial density was $\rho_0 = 1.66 \times 10^3 \text{ kg/m}^3$ ($\theta_w = 15^\circ, \phi_w = 11^\circ$), and the plug mechanism occurred in the initial stage of flow, the densities in the rigid-motion region and below were 1.53×10^3 and $1.49 \times 10^3 \text{ kg/m}^3$, respectively.

Measurements of the mass m of the material flowing out of the hopper model indicated that the flow rate dm/dt is constant through both the initial and advanced stages of flow. Neither the initial density nor the initial height of the material placed in the hopper was observed to have any influence on the flow rate. It is clear that the flow rate is strongly dependent on the width of the outlet. A decrease in the flow rate was observed when the half-angle θ_w or the wall friction angle ϕ_w was increased.

THEORETICAL DESCRIPTION OF ADVANCED FLOW

Theoretical description is restricted to the advanced stage of flow. A rigid-perfectly plastic model of granular material is adopted. The material is postulated to be isotropic and to obey the Mohr-Coulomb yield condition. The strain-rate tensor $\dot{\epsilon}_{ij}$ is related to the stress tensor σ_{ij} by the potential flow rule

$$\dot{\epsilon}_{ij} = \dot{\lambda} \frac{\partial G(\sigma_{ij})}{\partial \sigma_{ij}} \quad \dot{\lambda} > 0 \quad (1)$$

The potential function has a form similar to the Mohr-Coulomb yield condition, in which the angle of internal friction ϕ is replaced by the dilation angle ϕ^* ($0 < \phi^* < \phi$):

$$G(\sigma_x, \sigma_y, \tau_{xy}) = [(\sigma_x - \sigma_y)^2 + 4\tau_{xy}^2]^{1/2} + (\sigma_x + \sigma_y) \sin \phi^* \quad (2)$$

Compression is taken here in a negative sense. Using eqns. (1) and (2), and the geometrical relations

$$\dot{\epsilon}_{ij} = \frac{1}{2} \left(\frac{\partial V_i}{\partial x_j} + \frac{\partial V_j}{\partial x_i} \right) \quad i = 1, 2, 3 \quad (3)$$

for the plane flow in the plane $z = \text{const.}$ ($x = x_1, y = x_2, z = x_3$), the equations relating the velocity components V_x and V_y can be derived as

$$\begin{aligned} \left(\frac{\partial V_x}{\partial x} - \frac{\partial V_y}{\partial y} \right) \sin 2\psi - \\ - \left(\frac{\partial V_x}{\partial x} + \frac{\partial V_y}{\partial y} \right) \cos 2\psi = 0 \end{aligned} \quad (4)$$

$$\begin{aligned} \frac{\partial V_x}{\partial x} (\sin \phi^* - \cos 2\psi) - \\ - \frac{\partial V_y}{\partial y} (\sin \phi^* + \cos 2\psi) = 0 \end{aligned}$$

in which

$$\psi = \frac{1}{2} \arctan \frac{2\tau_{xy}}{\sigma_x - \sigma_y}$$

is the angle of inclination of the algebraically greater principal stress to the x -axis. Equations (4) are of a linear hyperbolic type, and can be solved by means of the method of characteristics [7]. The equations for the characteristics α and β are given as

$$\frac{dy}{dx} = \tan \left[\psi \pm \left(\frac{\pi}{4} + \frac{\phi^*}{2} \right) \right] \quad \alpha, \beta \quad (5)$$

and the projections of the velocity vector on the directions of lines α and β satisfy the following relations:

$$dV_\alpha - (V_\alpha \tan \phi^* + V_\beta \sec \phi^*) d\psi = 0 \quad \text{along } \alpha \quad (6)$$

$$dV_\beta + (V_\alpha \sec \phi^* + V_\beta \tan \phi^*) d\psi = 0 \quad \text{along } \beta$$

Equations (5) and (6) can be employed for solving a boundary value problem, provided that the angle ψ , as a function of x and y , is given. The field of ψ should be determined from a statical solution.

Strong or weak velocity discontinuities are admissible for the system (4). Experimentally observed rupture surfaces occurring within the flowing material will be identified here with the strong discontinuities of the velocity field. As shown by Shield [7], the velocity jump vector $[V]$ across the discontinuity line must be inclined to the discontinuity line at the angle ϕ^* . The change in velocity jump along the discontinuity line satisfies the following relation:

$$[V] = [V]_0 \exp[\pm(\psi - \psi_0) \tan \phi^*] \quad (7)$$

where $[V]_0$ is the known value of the velocity jump at a given point where $\psi = \psi_0$. The sign '+' in eqn. (7) should be used if the discontinuity appears along the α -characteristic, and the '-' sign for discontinuity along the β -characteristic.

Stresses in hoppers have been considered by many authors [9, 21, 22, 23, 24]. Generally, two methods of computing the stresses were postulated. The first one is based upon a differential slice analysis and gives only a prediction of wall pressures. The second method is based upon an assumption that a limiting stress field exists throughout the whole flowing area. The stress field within the material, pressure on the walls, and stresses along the outlet follow from the solution of a boundary value problem for a given stress condition along the top boundary of the material placed in the hopper. Such a solution was shown by Savage and Yong [23] for the active state and by Horne and Nedderman [24] for the passive state. The solution for the passive case obtained by Horne and Nedderman gives a discontinuous stress field. Unfortunately, it can not be adopted here since no effective method for solving the velocity problem coupled with a discontinuous stress field exists. A different approach, based on the idea of a radial stress field, was proposed earlier by Jenike [9]. Placing the origin of the polar co-ordinate system (r, θ) in the apex of the hopper, the distribution of the angle ψ was defined by Jenike as a function of θ only, and the mean normal stress as a product of the co-ordinate r ,

specific weight of the material γ , and an unknown function $\kappa(\theta)$. Finally, a set of two ordinary differential equations for $\psi(\theta)$ and $\kappa(\theta)$ is obtained. Although the radial stress field does not satisfy the boundary condition on the top surface, it seems to accurately approximate the stress distribution (on the average) on the walls and along the center line obtained by Horne and Nedderman (see [24]).

A continuous stress field for a given boundary condition along the outlet of the hopper was obtained by the author (see Fig. 6). The artificial boundary AA' was postulated to be circular and the external pressure p perpendicular to this boundary. The radius of the boundary AA' was chosen such that no stress singularity occurred at points A and A' . Starting the solution from the boundary AA' , the stress field above the outlet can easily be computed. For large values of p , stresses increase continuously with the distance from the outlet. However, for relatively small values of p , the stress components initially increase with the distance from the apex, then decrease, and finally vanish along a curvilinear contour. This contour can be interpreted as a free boundary of the material placed in the hopper. Small changes in the value of the boundary pressure p were found to affect the stress state very strongly in the whole flow area. The pattern of the principal stress directions, however, was affected only in a close vicinity of the boundary AA' . Since the obtained principal stress trajectories were very close to those given by Jenike [9], the radial

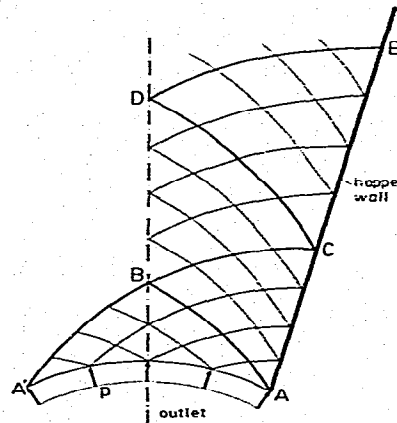


Fig. 6. Stress characteristics for a continuous stress field (passive case).

stress field is finally adopted in this paper. In order to determine the velocity field, the construction of a hodograph [25] will be used instead of numerical integration of eqns. (5) and (6).

A mesh of velocity characteristics based on the radial stress field is shown in Fig. 7a) ($\theta_w = 15^\circ$, $\phi = 32^\circ$, $\phi_w = 11^\circ$, $\phi^* = 10^\circ$). Although the flow is non-stationary, the mesh of characteristics resulting from the radial stress field is time-independent. The non-steady character of the process will be reflected in the variation of the boundary conditions with time. Referring to the experimental results, the area ABC is assumed to move as a rigid body parallel to the wall with velocity V_0 . The symmetry of the problem requires the velocity vector just below point B to be vertical. Hence, the characteristic BC is the velocity discontinuity line, and the velocity jump vector along BC can be computed from eqn. (7). Next, the boundary value problem for velocities can be solved in region BCD. The characteristic CD is the next velocity discontinuity line. The velocity jump along CD can be determined from eqn. (7), and the boundary value problem for velocities can be solved in the region CDE. Solution for the velocities in the area DEF is then similar to that in BCD, etc. Figure 7b) shows the hodograph corresponding to the mesh of characteristics in Fig. 7a). It can be easily

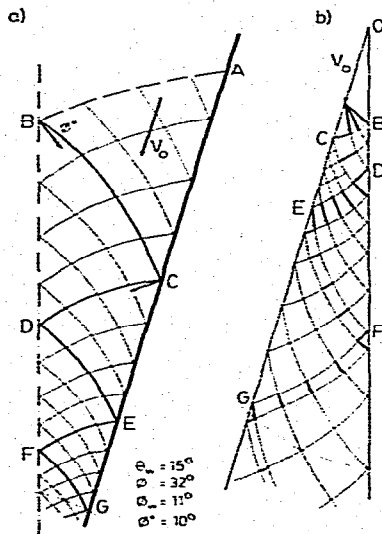


Fig. 7. Velocity characteristics mesh based on the radial stress field (a)) and the hodograph (b)).

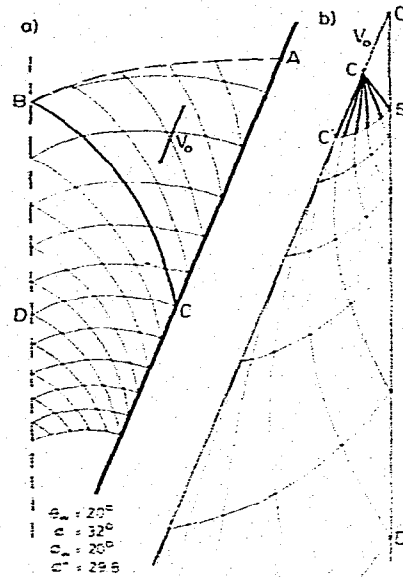


Fig. 8. The case with only one discontinuity line in the velocity field. Mesh of velocity characteristics (a)), hodograph (b)).

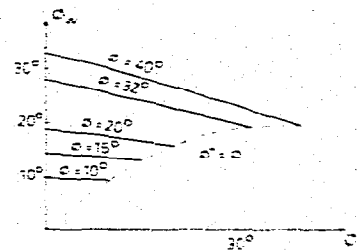


Fig. 9. Material parameters for which only one discontinuity line occurs in the velocity field.

shown that for some combinations of the parameters ϕ , ϕ^* and θ_w , the velocity jump vector at point C is collinear with V_0 and line BC is the only discontinuity in the velocity field (see Fig. 8). Material parameters for which only one discontinuity occurs in the velocity field are represented by the diagrams in Fig. 9.

An incompressible flow below the most upper velocity discontinuities was experimentally observed. Consequently, the solution for $\phi^* = 0$ rather than $\phi^* > 0$ is expected to be in better agreement with experimental measurements. Results obtained by Pariseau [1], based upon the assumption of incompressibility, were also found to match the experiments better than those corresponding to dilatant material.

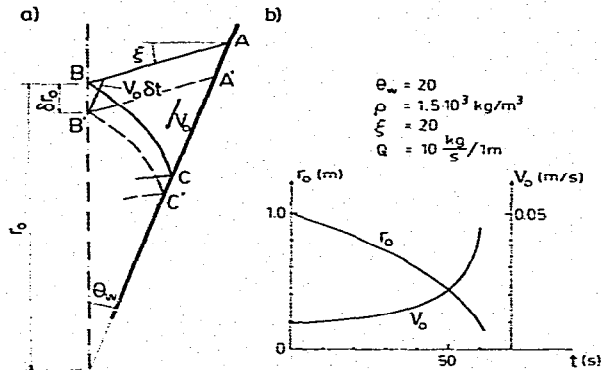


Fig. 10. Variation of the characteristic dimension δr_0 due to a time increment δt (a); characteristic dimension r_0 and velocity V_0 as functions of time (b).

The above kinematic solution provides a non-negative rate of dissipated work within the flowing material.

The hodographs in Fig. 7b) and Fig. 8b) represent the velocity fields at a certain time t . However, the geometry of the hodograph remains similar at any time t since the mesh of velocity characteristics is time-independent. Hence, the flow can be described as a pseudo-steady process. This is confirmed by the experimental results, which show that discontinuity lines are geometrically similar throughout the advanced stage of flow. The pseudo-steady character of the flow would be preserved rigorously if the whole flow pattern was geometrically similar throughout the process of discharge. It is obvious, however, that the width of the outlet is fixed, and thus, some departure from the pseudo-steady character of the flow must occur. Therefore, the solution is restricted only to the flow area inside the hopper and can be applied until the rigid-motion regions reach the outlet level.

In the above solution, the velocity V_0 is unknown. V_0 can be evaluated, however, if the flow rate Q and the characteristic dimension r_0 (see Fig. 10a) are known. In view of the experimental results, it is reasonable to assume a constant rate of mass discharge Q . Assuming further, for simplicity, that the free boundary of the material is a straight line, inclined at an angle ξ to the horizon, the relation between the variation of the characteristic dimension δr_0 and velocity V_0 , corresponding to a time increment δt , and the relation between Q and V_0 can both be derived from the continuity condition and

the principle of mass conservation (see geometrical relations in Fig. 10a)):

$$\delta r_0 = V_0 \frac{\cos(\xi + \theta_w)}{\cos \xi} \delta t \quad (8)$$

$$Q = \rho \left[2V_0 r_0 - V_0^2 \frac{\cos(\xi + \theta_w)}{\cos \xi} \delta t \right] \sin \theta_w \quad (9)$$

Equation (9) is valid for an incompressible material with a uniform density ρ . Q is the mass flow rate per unit dimension perpendicular to the plane of flow. Figure 10b) shows the variation of V_0 and r_0 with time, obtained from eqns. (8) and (9) for certain assumed values of Q , θ_w , ρ and ξ .

It was assumed for simplicity that the free boundary of the material is a straight line. Assuming a more real, curvilinear shape of the boundary, eqns. (8) and (9) have more complicated forms, but the hodograph remains unaltered.

Comparison of theoretical predictions with experimental results

In Fig. 11a, b), and c), the dimensionless radial components of the velocities of particles V_r/V_0 are shown as functions of a dimensionless distance from the apex of the hopper

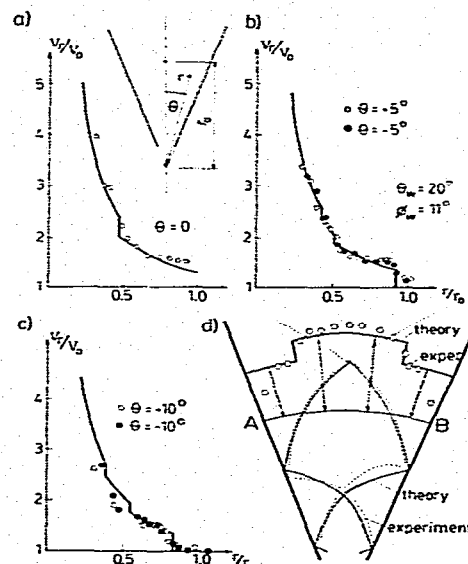


Fig. 11. Radial velocity components versus distance from the apex of the hopper (a) - c)) and the pattern of discontinuity lines (d)), for a hopper with half-angle $\theta_w = 20^\circ$ and $\phi = 32^\circ$, $\phi_w = 11^\circ$, $\rho_0 = 1.6 \times 10^3$ kg/m³.

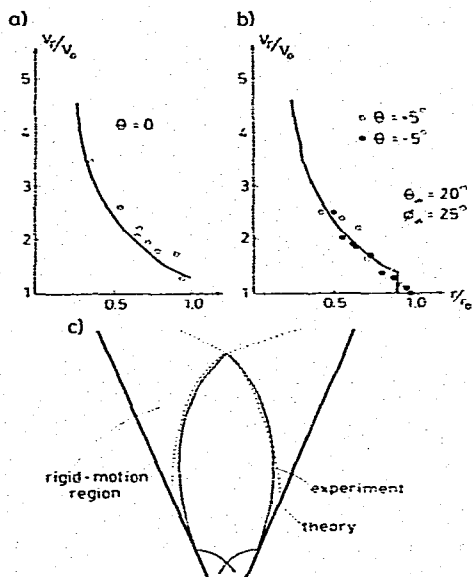


Fig. 12. Radial velocity components *versus* distance from the apex (a), b)) and the pattern of discontinuity lines (c)), for a hopper with half-angle $\theta_w = 20^\circ$ and $\phi = 32^\circ$, $\phi_w = 25^\circ$, $\rho_0 = 1.6 \times 10^3 \text{ kg/m}^3$.

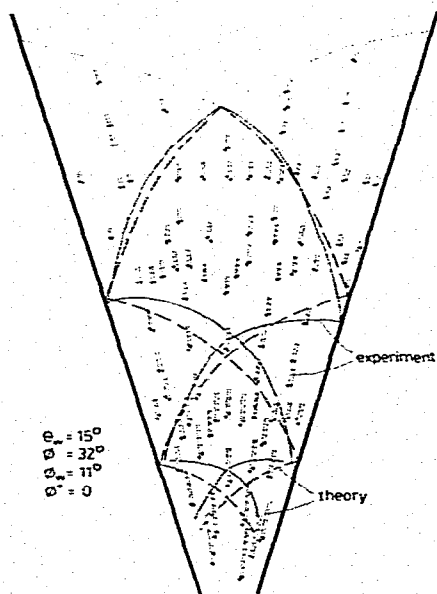


Fig. 13. Velocity vectors and discontinuity lines determined from experiments and theoretical predictions ($\theta_w = 15^\circ$, $\phi = 32^\circ$, $\phi_w = 11^\circ$).

r/r_0 . The circles represent the experimentally obtained results, whereas the solid lines pertain to theoretical values. The experimental results in Fig. 11 refer to a hopper

with half-angle $\theta_w = 20^\circ$, wall friction angle $\phi_w = 11^\circ$ and initial density $\rho_0 = 1.6 \times 10^3 \text{ kg/m}^3$. Theoretical results (solid line) were obtained under the assumption of incompressibility of the flow and for the angle $\phi = 32^\circ$, as measured in a triaxial test. The shape of the discontinuities in the velocity field and the velocity distribution along the arc AB are shown in Fig. 11d). The results for the same hopper, but with $\phi_w = 25^\circ$, are shown in Fig. 12.

A comparison of the experimentally measured and theoretically predicted particle velocities and location of the velocity discontinuity lines for a hopper model with half-angle $\theta_w = 15^\circ$ and wall friction angle $\phi_w = 11^\circ$ is shown in Fig. 13.

The results shown in Figs. 11, 12 and 13 indicate fairly good agreement between the theoretical solution and experimental observations.

CONCLUSIONS

The velocity field was experimentally determined in a wedge-shaped hopper model containing dry sand, and an attempt towards a theoretical description of the advanced stage of flow was carried out.

Mass flow or plug flow mechanisms are likely to appear in the initial stage of flow. In both mechanisms, distinct narrow zones of large shear deformation (velocity discontinuities), accompanied by dilation of the material, are present. After the initial stage of flow is completed, the entire material starts to move and the pattern of the velocity discontinuities becomes geometrically similar throughout the advanced stage of flow. The flow rate appears to be constant in both initial and advanced stages of flow.

A theoretical description of the kinematics of the advanced flow, based upon the plane plastic flow theory of incompressible material, coupled with the radial stress field, seems to accurately describe the real velocity field, particularly in hoppers with smooth walls. A pseudo-steady mechanism is suggested for the advanced stage of flow. A similar strategy of solving kinematics in hoppers was proposed earlier by Pariseau [1]. However, in the latter paper, the directions of principal strain rates were determined experimentally, and bound-

ary conditions for velocities differed from those proposed in this paper. The description proposed here gives results similar to those obtained by Drescher, Cousens and Bransby [11], who assumed the presence of only one pair of discontinuity lines in the velocity field. This approximation seems to be reasonable since the jump in the velocity vectors across the other discontinuities is relatively small, as demonstrated in the present paper.

This paper was focused only on a small part of the problems associated with flow of granular cohesionless materials through hoppers. Although the existence of discontinuities in the velocity field was reported previously by other authors, the observations of their development presented in this paper contribute to a better understanding of the kinematics of the flow process. Comparison of the mathematical description of the advanced flow presented in the paper with experimental results allows one to believe that the rigid-perfectly plastic model is a good approximation for granular material in advanced flow. The formulation of a velocity boundary value problem in the initial stage of flow remains a subject of research. It is believed that in this stage of flow only part of the material in the hopper experiences plastic deformation, and therefore traditional plastic flow theory does not seem to be a promising framework of analysis.

ACKNOWLEDGEMENTS

The Author would like to thank Professor A. Drescher for his helpful advice and for allowing the use of his X-radiographs in this paper. The Author is also grateful to the Council for International Exchange of Schol-

ars for financial support while doing research at the University of Minnesota.

REFERENCES

- 1 W. G. Pariseau, *Powder Technol.*, 3 (1970) 218.
- 2 P. M. Blair-Fish and P. L. Bransby, *J. Engng. Ind., Trans. ASME, Ser. B*, 95 (1973) 17.
- 3 P. L. Bransby and P. M. Blair-Fish, *Powder Technol.*, 11 (1975) 273.
- 4 J. Lee, S. C. Cowin and J. S. Templeton, *Trans. Soc. Rheol.*, 18 (1974) 247.
- 5 R. M. Nedderman and U. Tüzün, *Powder Technol.*, 22 (1979) 243.
- 6 U. Tüzün and R. M. Nedderman, *Powder Technol.*, 31 (1982) 27.
- 7 R. T. Shield, *Q. Appl. Math.*, 11 (1953) 61.
- 8 R. T. Shield, *J. Mech. Phys. Solids*, 3 (1955) 246.
- 9 A. W. Jenike, *Gravity Flow of Bulk Solids*, *Bull. Univ. Utah* 108, vol. 52 (1961).
- 10 A. J. M. Spencer, *J. Mech. Phys. Solids*, 12 (1964) 337.
- 11 A. Drescher, T. W. Cousens and P. L. Bransby, *Géotechnique*, 28 (1978) 27.
- 12 J. Litwiniszyn, *Bull. Acad. Pol. Sci.*, 11 (1963) 593.
- 13 W. W. Mullins, *J. Appl. Phys.*, 43 (1972) 665.
- 14 W. W. Mullins, *Powder Technol.*, 23 (1979) 115.
- 15 P. L. Bransby, P. M. Blair-Fish and R. G. James, *Powder Technol.*, 8 (1973) 197.
- 16 J. O. Cutress and R. F. Pulfer, *Powder Technol.*, 1 (1967) 213.
- 17 R. Butterfield, R. Harkness and K. Andrawes, *Géotechnique*, 20 (1970) 308.
- 18 R. G. James, *Report No. CUED/C-Soils/LNI (1973)*, Engng. Dept. University of Cambridge.
- 19 B. O. Hardin and F. E. Richart, Jr., *Proc. ASCE*, 89 (1963) SM1, 33 - 65.
- 20 E. Drescher and R. Michalowski, *Mech. Teoret. Stos.*, 17 (1979) No. 3 (in Polish) 441.
- 21 D. M. Walker, *Chem. Eng. Sci.*, 21 (1966) 975.
- 22 J. K. Walters, *Chem. Eng. Sci.*, 28 (1973) 779.
- 23 S. B. Savage and R. N. Yong, *Int. J. Mech. Sci.*, 12 (1970) 675.
- 24 R. M. Horne and R. M. Nedderman, *Powder Technol.*, 19 (1978) 243.
- 25 A. P. Green, *J. Mech. Phys. Solids*, 2 (1954) 73.